

Kriging interpolating cosmic velocity field. II: Taking anisotropies and multi-streaming into account

Yu Yu,^{1,*} Jun Zhang,^{2,3} Yipeng Jing,^{2,3} and Pengjie Zhang^{2,3,1,†}

¹*Key laboratory for research in galaxies and cosmology, Shanghai Astronomical Observatory, Chinese Academy of Sciences, 80 Nandan Road, Shanghai 200030, China*

²*Center for Astronomy and Astrophysics, Department of Physics and Astronomy, Shanghai Jiao Tong University, 200240, Shanghai*

³*IFSA Collaborative Innovation Center, Shanghai Jiao Tong University, Shanghai 200240, China*

Measuring the volume-weighted peculiar velocity statistics from inhomogeneously and sparsely distributed galaxies/halos, by existing velocity assignment methods, suffers from a significant sampling artifact. As an alternative, the Kriging interpolation based on Gaussian processes was introduced and evaluated [Y. Yu, J. Zhang, Y. Jing, and P. Zhang, Phys. Rev. D 92, 083527 (2015)]. Unfortunately, the most straightforward application of Kriging does not perform better than the existing methods in the literature. In this work, we investigate two physically motivated extensions. The first takes into account of the anisotropic velocity correlations. The second introduces the nugget effect, on account of multi-streaming of the velocity field. We find that the performance is indeed improved. For sparsely sampled data [$n_P \lesssim 6 \times 10^{-3} (h^{-1} \text{Mpc})^{-3}$] where the sampling artifact is the most severe, the improvement is significant and is two-fold: 1) The scale of reliable measurement of the velocity power spectrum is extended by a factor ~ 1.6 , and 2) the dependence on the velocity correlation prior is weakened by a factor of ~ 2 . We conclude that such extensions are desirable for accurate velocity assignment by Kriging.

PACS numbers: 98.80.-k, 95.36.+x, 98.80.Bp

I. INTRODUCTION

Peculiar velocity of galaxies and other tracers of the large-scale structure such as free electrons and 21 cm emitting neutral hydrogen atoms probes the structure growth rate of the Universe. It is therefore a valuable probe of dark matter, dark energy and gravity at cosmological scales (e.g., Refs. [1–15]). It also offers the possibility of probing horizon-scale inhomogeneities of the Universe and therefore tests the external inflation [16, 17]. In different circumstances, the measured velocity statistics can have different weighting. For example, the kinetic Sunyaev-Zel’dovich effect is proportional to the gas momentum, which is the gas density-weighted velocity. On the other hand, one can infer the volume-weighted velocity power spectrum from redshift space distortions (RSD), by comparing the measured RSD power spectrum with the theoretical modelling. In this approach, the RSD theory models the volume-weighted velocity statistics (e.g., Ref. [18]).

The density-weighted velocity statistics suffers from the problem of density bias, which is hard to calculate from the first principle. In contrast, the volume-weighted velocity statistics is free of this problem. Therefore, for the purpose of precision cosmology, it is more desirable than the density-weighted velocity statistics. For this aspect, RSD cosmology requires accurate understanding of the volume-weighted velocity statistics. Due to the non-linear evolution of the large-scale structure, the most ro-

bust way of understanding the volume-weighted velocity statistics is through cosmological simulations. Through them, we can measure the velocity statistics of simulation particles, halos and mock galaxies.

However, accurate measurement of the volume-weighted velocity in simulations is nontrivial, due to the very fact that we only sample the velocity field where there are simulation particles (e.g., Refs. [19–25]). Since the particle distribution is inhomogeneous and since it is correlated with the signal (velocity) that we aim to measure, the sampling of the velocity field is biased. This sampling artifact increases with decreasing the sample number density n_P (e.g., [23]). It is already detectable for $n_P \sim 1 \text{Mpc}^{-3}$ [21]. For sparse samples such as massive halos, the problem is much more severe. For example, when $n_P \sim 10^{-4} \text{Mpc}^{-3}$, the induced error in the velocity power spectrum increases to $\mathcal{O}(10)\%$, even at scales as large as $k = 0.1 h/\text{Mpc}$ [24].

To solve/alleviate this long-standing problem, several methods of velocity assignment have been proposed:

- (1) The Voronoi tessellation (VT) method [19] is a zeroth-order interpolation scheme. One constructs the Voronoi tessellation from a set of nodes (i.e., particles/halos). The velocity inside a tessellation element (i.e., the Voronoi polyhedral) is approximated as the velocity of the only particle enclosed. One then obtains the velocity on regular grids by smoothing this space-filling velocity field.
- (2) The Delaunay tessellation (DT) method [20] is a linear interpolation scheme. One first constructs the Delaunay tessellation, which is the dual of Voronoi tessellation. One then approximates the

* yuyu22@shao.ac.cn

† zhangpj@sjtu.edu.cn

velocity gradient inside a Delaunay tessellation element (i.e., the Delaunay tetrahedron) as a constant, determined by the velocities of the four vertices. The two steps construct the velocity field at all positions. One can then apply a smoothing onto the interpolated velocity field.

- (3) In the works by Zheng *et al.* [21] and Koda *et al.* [22], the nearest-particle (NP) method was proposed and applied. It assigns the velocity of a regular grid point as the velocity of the nearest particle to it. It is essentially the VT method without smoothing.

Zhang *et al.* [23] studied the sampling artifact theoretically and verified the theoretical modelling through simulations [24]. One finding is that the polynomial interpolation has to be at least quadratic, in order to be free of the leading-order sampling artifact. Therefore, sampling artifacts of the above velocity assignment methods are all severe for sparse samples, consistent with the simulation tests of the NP method [24] and the DT method [25].

This motivates us to try alternative methods. In our previous work [26] (hereafter paper I), the Kriging method was introduced and tested. The Kriging interpolation, originally used in geostatistics, is an application of Gaussian processes. It assumes the Gaussian distribution for the field to be interpolated. With a set of positions with known field values (data) and adopting priors on the spatial correlation function of the field, the posterior distribution of the field value at any other spatial location can be predicted. Kriging then assigns the peak value of such posterior distribution as the field value at the given position. Therefore, Kriging is a maximum likelihood estimator. Furthermore, one can prove that this peak value is the weighted linear combination of field values of nearby positions [Eq. 3], and the resulting error dispersion is minimal (a detailed explanation can be found in paper I). Therefore it is also a minimal variance linear estimator. Actually, this provides the most straightforward viewpoint of Kriging and leads to the most direct derivation of the Kriging formula presented in paper I and in the current paper.

However, despite the above desirable properties, we found that the versions of Kriging investigated in paper I do not perform better than the NP method for reconstructing the 3D velocity field on regular grids. In Kriging, 2 degrees of freedom in Kriging can be explored to improve its performance: 1) One can choose the set of positions with known values to perform the interpolation. For example, one can use the n_k particles nearest the given point, and in the limiting case of $n_k = 1$, it reduces to the NP method. Since the particle distribution is inhomogeneous, the spatial range of interpolation varies from position to position [27]. Paper I has investigated the cases of $n_k = [10, 200]$. 2) Another degree of freedom is the priors on the spatial correlation function of the field. Paper I fixed the velocity correlation function as that predicted by the Lambda cold dark matter

(Λ CDM) cosmology while trying two different values of Ω_m . When the sample density is low, the performance of Kriging is sensitive to the adopted priors (paper I). This motivates us to adopt priors of better physical motivations.

One motivation is that the physical velocity correlation function $\xi_{\alpha\beta}(\mathbf{r})$ between the α th component at position \mathbf{r}_1 and the β th component at position \mathbf{r}_2 is anisotropic. Namely $\xi_{\alpha\beta}(\mathbf{r}) \equiv \langle v_\alpha(\mathbf{r}_1)v_\beta(\mathbf{r}_2) \rangle$ depends on not only the amplitude of the separation vector $\mathbf{r} \equiv \mathbf{r}_2 - \mathbf{r}_1$ but also on its direction $\hat{r} \equiv \mathbf{r}/r$. In fact, it can be decomposed into two isotropic correlation functions $\psi_\perp(r)$ and $\psi_\parallel(r)$ [28],

$$\xi_{\alpha\beta}(\mathbf{r}) = \psi_\perp(r)\delta_{\alpha\beta} + [\psi_\parallel(r) - \psi_\perp(r)]\hat{r}_\alpha\hat{r}_\beta. \quad (1)$$

Here, $\alpha, \beta = x, y, z$ indicates the three Cartesian axes. $\delta_{\alpha\beta}$ is the Kronecker delta function. Figure 1 shows $\psi_{\perp, \parallel}(r)$ in a Λ CDM universe. The two show visible inequality, meaning significant anisotropy in $\xi_{\alpha\beta}(\mathbf{r})$, as shown in Fig. 2. Paper I ignored such anisotropy and adopted the averaged correlation function $\xi_{vv} \equiv \langle \mathbf{v}(\mathbf{r}_1) \cdot \mathbf{v}(\mathbf{r}_2) \rangle = (\psi_\parallel + 2\psi_\perp)/3$. Since the anisotropy is $\mathcal{O}(10)\%$ at $r = 10h^{-1}\text{Mpc}$ and can be even larger at larger r , this is expected to result in significant error in the reconstructed velocity field.

Other physics missing in paper I are the multistreaming of the velocity field. In the late stage of structure formation, shell crossing develops, and the velocity field is no longer single valued. This means that, even when two particles share the same position, they may not share the same velocity. In terms of the correlation function,

$$\langle v_\alpha^2 \rangle - \xi_{\alpha\alpha}(r \rightarrow 0) \neq 0. \quad (2)$$

In the language of Kriging, this corresponds to a variogram nonzero at $r = 0$, namely, the nugget effect. Paper I ignored this complexity. In the current paper, we will take it into account and test whether it can improve the Kriging performance.

For clarity, we call the Kriging investigated in paper I “Kriging I” and the version considering anisotropies and multi-streaming of the velocity field “Kriging II”. This paper is organized as follows. In Sec. II, we briefly introduce the general idea of Kriging, Kriging I, and Kriging II. In Sec. III, we briefly describe the simulation and velocity statistics we use. In Sec. IV, we present the performance test of Kriging II. We conclude and discuss in Sec. V.

II. KRIGING INTERPOLATION AS A VELOCITY ASSIGNMENT METHOD

A. General idea of Kriging

We want to estimate the field value y_* at a given position \mathbf{x}_* based on the n_k points at \mathbf{x}_i with observed values

$y_i = y(\mathbf{x}_i)$. Kriging predicts y_* as a weighted linear combination of y_i ,

$$y_* = \sum_i W_i y_i. \quad (3)$$

Here, the weighting W_i depends on the position \mathbf{x}_i , but not on y_i . It satisfies the unbiased condition $\sum_i W_i = 1$. By minimizing the rms error with respect to the data, the weighting \mathbf{W} is determined. Therefore, Kriging relies on the *variogram* of the field,

$$\begin{aligned} \gamma(\mathbf{r}) &= \frac{1}{2} \langle [y(\mathbf{x} + \mathbf{r}) - y(\mathbf{x})]^2 \rangle, \\ &= \langle y^2 \rangle - \langle y(\mathbf{x} + \mathbf{r})y(\mathbf{x}) \rangle. \end{aligned} \quad (4)$$

With the variogram prior specified, the weighting \mathbf{W} is solved from the following Kriging system:

$$\begin{bmatrix} \mathbf{W} \\ \mu \end{bmatrix} = \begin{bmatrix} \gamma_{ij} & \mathbf{1} \\ \mathbf{1}^T & 0 \end{bmatrix}^{-1} \begin{bmatrix} \gamma_{i*} \\ 1 \end{bmatrix}. \quad (5)$$

Here, γ_{ij} is the matrix containing the variogram values between observed points, with $\gamma_{ij} \equiv \gamma(\mathbf{x}_i - \mathbf{x}_j)$. It has a dimension of $n_k \times n_k$. Unity vector $\mathbf{1}^T$ is set for the unbiased condition $\sum_i W_i = 1$. The vector $\gamma_{i*} \equiv \gamma(\mathbf{x}_i - \mathbf{x}_*)$. μ is the Laplacian multiplier. We refer the readers to the Appendix of paper I for the derivation of the Kriging system.

B. Kriging I

To proceed, we need to adopt a variogram. Kriging I of paper I makes two simplifications. Kriging I adopts the direction-averaged variogram from linear theory and therefore neglects the anisotropic in the velocity field. The adopted variogram is given by $\gamma(r) = 1 - \xi_{vv}(r)/\xi_{vv}(0)$. Here, $\xi_{vv}(r) \equiv \langle \mathbf{v}(\mathbf{r}_1) \cdot \mathbf{v}(\mathbf{r}_2) \rangle$, with no dependence on the direction of \mathbf{r} .

This choice of variogram automatically satisfies $\gamma(r \rightarrow 0) \rightarrow 0$. Under such a condition, $y(\mathbf{x}_* \rightarrow \mathbf{x}_i) \rightarrow y_i$. Namely, Kriging honors the observed values at observed positions. The condition $\gamma(r \rightarrow 0) \rightarrow 0$ is satisfied as long as the field is single valued.

However, in reality, the velocity correlation function is anisotropic, and the velocity field is multi-valued in some regions such as halos. Therefore, we propose Kriging II to improve the velocity assignment.

C. Kriging II

The anisotropic velocity correlation function has the general form of Eq. (1), with two functions $\psi_{\parallel, \perp}(r)$. At large scales of interest, the velocity field is curl free. We then have the textbook result [28]

$$\psi_{\perp}(r) = 3H^2 \int \frac{dk}{k} \frac{\Delta_{\theta\theta}^2}{k^2} \left[\frac{\sin(kr)}{(kr)^3} - \frac{\cos(kr)}{(kr)^2} \right], \quad (6)$$

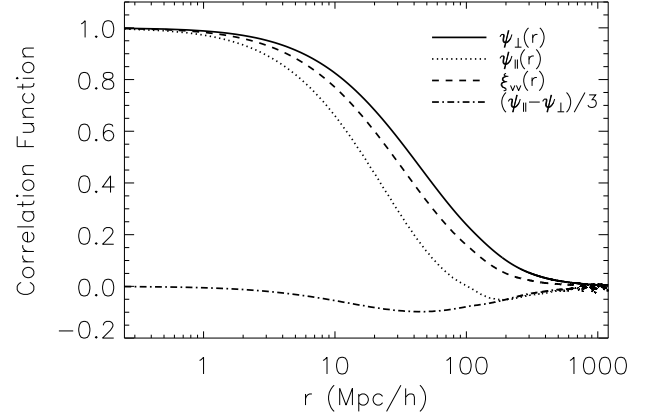


FIG. 1. The theoretically predicted two velocity correlation functions $\psi_{\perp}(r)$ (solid line) and $\psi_{\parallel}(r)$ (dotted line) that form the anisotropic velocity correlation function [Eq. (1)]. The direction-averaged velocity correlation function adopted in Kriging I is presented by the dashed line. The direction-averaged velocity correlation between different velocity components is presented by the dot-dashed line.

$$\psi_{\parallel}(r) = 3H^2 \int \frac{dk}{k} \frac{\Delta_{\theta\theta}^2}{k^2} \left[\frac{\sin(kr)}{kr} - 2 \frac{\sin(kr)}{(kr)^3} + 2 \frac{\cos(kr)}{(kr)^2} \right]. \quad (7)$$

Here, H is the Hubble parameter, and $\Delta_{\theta\theta}^2(k) = k^3 P_{\theta\theta}(k)/2\pi^2$ is the velocity divergence power spectrum. ψ_{\parallel} and ψ_{\perp} are not independent. The two satisfy the following consistency relation:

$$\psi_{\parallel}(r) = \frac{d(r\psi_{\perp}(r))}{dr}. \quad (8)$$

Theoretically predicted (normalized) ψ_{\perp} and ψ_{\parallel} based on Λ CDM cosmology are presented in Fig. 1. The two differ significantly. It results in the anisotropic velocity correlation function $\xi_{xx}(\mathbf{r})$ and $\xi_{xy}(\mathbf{r})$ (Fig. 2). The shown anisotropy implies that, to interpolate one specific velocity component, the optimal weighting should differ for particles at the same r but different \hat{r} . It also implies that for a fixed position, the weighting for different velocity components is different.

In principle, we can construct v_{α} from v_{β} with $\beta \neq \alpha$, for the reason that $\xi_{\alpha\beta} \neq 0$. However, since the correlation when $\alpha \neq \beta$ is in general much weaker than the case of $\alpha = \beta$ (Fig. 2), the reconstruction is the most accurate for the case of $\alpha = \beta$. Hereafter, we will only consider this case; namely, we interpolate v_{α} at some given positions to obtain v_{α} at other positions. The corresponding variogram, normalized at $r = 0$, is

$$\begin{aligned} \gamma_{\alpha\alpha}(\mathbf{r}) &\equiv 1 - \xi_{\alpha\alpha}(\mathbf{r})/\xi_{\alpha\alpha}(0), \\ &= \gamma_{\perp}(r) + [\gamma_{\parallel}(r) - \gamma_{\perp}(r)]\hat{r}_{\alpha}^2. \end{aligned} \quad (9)$$

Here, $\gamma_{\perp}(r) \equiv 1 - \psi_{\perp}(r)/\psi_{\perp}(0)$, and $\gamma_{\parallel}(r) \equiv 1 - \psi_{\parallel}(r)/\psi_{\parallel}(0)$.

An implicit assumption in the above results is that the velocity field has no multi-streaming, namely, is single

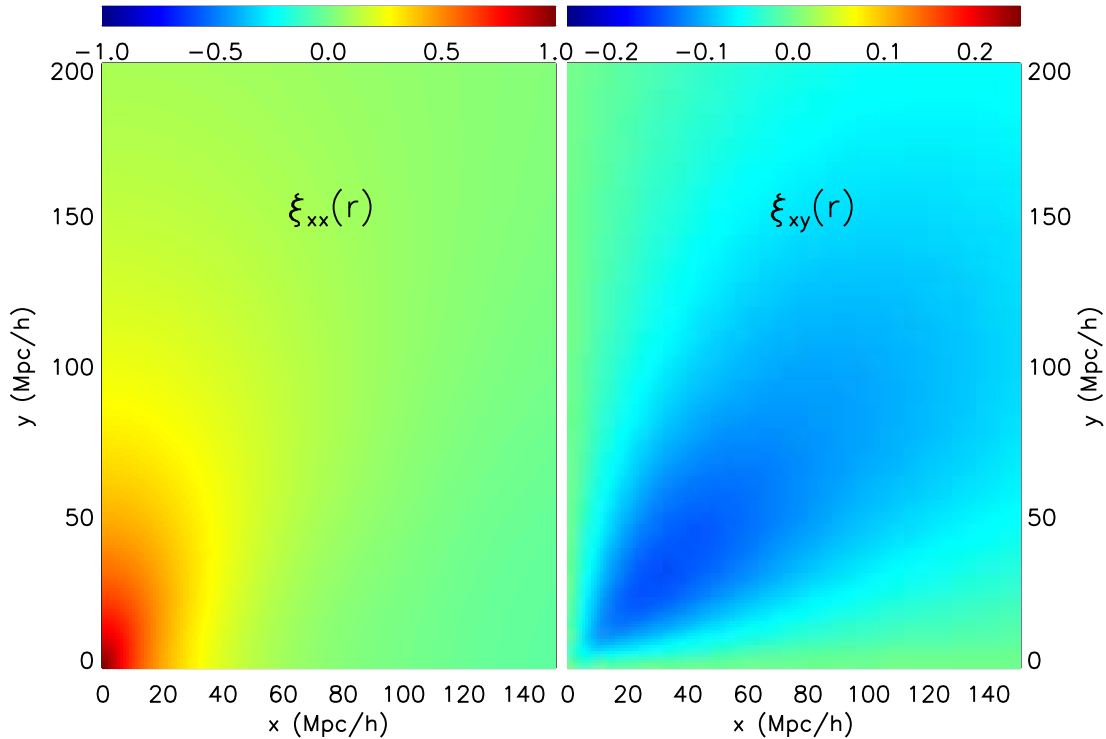


FIG. 2. The theoretically predicted normalized velocity correlation function between the same components [e.g., $\xi_{xx}(\mathbf{r})$] and between different components [e.g., $\xi_{xy}(\mathbf{r})$] is presented in the left and right panels, respectively. Strong anisotropy can be seen in the two velocity correlation functions. For the x velocity component, the correlation $\xi_{xx}(\mathbf{r})$ is stronger in the perpendicular y direction and relatively weaker in the parallel x direction. Notice that the two panels adopt different color scales to better present the anisotropy.

valued. So, it automatically satisfies $\gamma_{\alpha\alpha}(r \rightarrow 0) = 0$. Although this is a desirable property for some cases, it is inappropriate when there exist measurement errors or the true field itself is multi-valued. Since in this paper we restrict to simulations, we can neglect the measurement error. But in simulations, the velocity field is indeed multi-valued (multi-streaming), due to the nonlinear evolution induced shell crossing. For example, in massive clusters, particle motions are randomized, and we no longer have a single-valued velocity field. This results in $\gamma(r \rightarrow 0) \neq 0$ (the *nugget* effect). To model this effect, we introduce a dimensionless free parameter γ_{nug} and modify the variogram in Eq. (9) as

$$\gamma_{\alpha\alpha} \rightarrow \left[1 - \frac{\xi_{\alpha\alpha}(\mathbf{r})}{\xi_{\alpha\alpha}(0)} \right] + \gamma_{\text{nug}}. \quad (10)$$

It can be rewritten as $\gamma_{\alpha\alpha} = (1 + \gamma_{\text{nug}})(1 - \xi_{\alpha\alpha}(\mathbf{r})/(\xi_{\alpha\alpha}(0)(1 + \gamma_{\text{nug}})))$. Since Kriging does not depend on the overall amplitude of the variogram, the modification [Eq. (10)] is equivalent to $\xi_{\alpha\alpha}(0) \rightarrow \xi_{\alpha\alpha}(0)(1 + \gamma_{\text{nug}})$.

We then Kriging interpolate the velocity field for each velocity component with the corresponding variogram ($\alpha = x, y, z$),

$$v_{\alpha,*} = \sum_i W_{\alpha,i} v_{\alpha,i}. \quad (11)$$

Due to the anisotropic velocity correlation, $\mathbf{W}_x \neq \mathbf{W}_y \neq \mathbf{W}_z$. This is different from the case of isotropic velocity correlation, in which $\mathbf{W}_x = \mathbf{W}_y = \mathbf{W}_z$. Thus, in Kriging II, we need to solve the Kriging system for each individual component. The computational expense is tripled compared to Kriging I.

III. SIMULATION SPECIFICATION

A. Simulation

We test the performance of Kriging II using the same simulation data used in paper I to test Kriging I. The simulation is run by a particle-particle-particle-mesh code adopting the standard flat Λ CDM model, with cosmological parameters $\Omega_m = 0.268$, $\Omega_\Lambda = 0.732$, $\sigma_8 = 0.85$, $n_s = 1$, and $h = 0.71$ (see Ref. [29]). The dark matter particle number is 1024^3 , and the box size is $1200h^{-1}\text{Mpc}$.

We adopt the same trick as in Kriging I to test Kriging II. The sampling artifact vanishes in the limit of infinite particle number density. As the consequence, the full simulation sample with 1024^3 simulation particles and the NP [21] velocity assignment method robustly predicts the E-mode velocity power spectrum at scales of interest

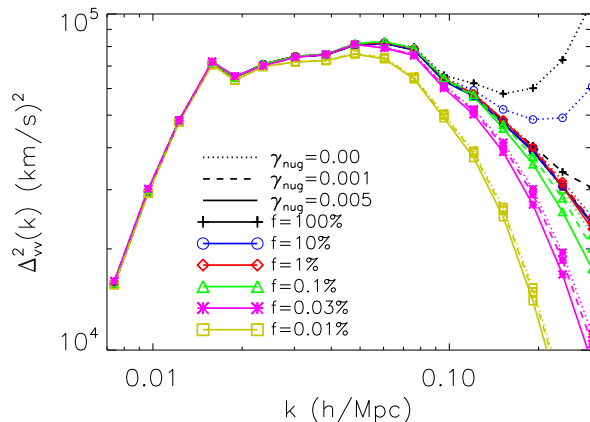


FIG. 3. E-mode velocity power spectrum from the Kriging method in which we arbitrarily choose the nugget values $\gamma_{\text{nug}} = 0, 0.001$, and 0.005 (dotted, dashed, and solid lines, respectively). For $f = 100\%$ and 10% , the estimated power without the nugget effect is boosted up in small scales, due to the instability in the Kriging system. Taking the nugget effect into consideration alleviates this problem but smooths the power a little in small scales.

($k \lesssim 0.1 h\text{Mpc}^{-1}$; see paper I). Therefore, we treat such a result as the reference. We then construct low number density samples by randomly selecting a fraction of f ($f = 10\%, 1\%, 0.1\%, 0.03\%, 0.01\%$) particles from the simulation. The number density of these samples scales with f as

$$n_P = \frac{1024^3}{1200^3} f (h^{-1}\text{Mpc})^{-3} = 0.62 f (h^{-1}\text{Mpc})^{-3}. \quad (12)$$

These samples have decreasing number density and therefore an increasing sampling artifact. In particular, future spectroscopic surveys such as Euclid [30], DESI [31], and PFS [32] will have a galaxy number density comparable to that of $f = 0.1\%$. Thus, the performance of Kriging II in this range of f is of particular interest. Comparing to paper I, we add $f = 0.03\%$ in this work, since Kriging I degrades significantly between $f = 0.1\%$ and 0.01% (see paper I).

We construct the velocity field on 256^3 uniform grid by Kriging II, using the n_k simulation particles nearest to a given grid point. The corresponding grid size is $4.7 h^{-1}\text{Mpc}$, safe for the scales of interest ($k \sim 0.1 h\text{Mpc}^{-1}$). In principle, we may use as many simulation particles as possible for Kriging. But in reality, we only need a very limited fraction of them. One reason is that only nearby particles have a non-negligible contribution in the Kriging interpolation. Distant particles have very weak correlation with the velocity of the given grid point. They have no contribution in Kriging. Another reason is that in dense regions, only a small amount of particles is needed for accurate interpolation. Following studies in paper I, $n_k = 200$ is sufficient for the purpose of our study. Thus, in this work, we fix $n_k = 200$ for all the cases.

B. Statistics

We restrict the test to the velocity E-mode power spectrum, which contains most of the cosmological information. Any vector field can be decomposed into an E-mode (gradient) and a B-mode (curl) component. We decompose the velocity field on the uniform grid points into an E-mode and a B-mode component by using a fast Fourier transform,

$$\mathbf{v}_E(\mathbf{k}) = \frac{(\mathbf{v}(\mathbf{k}) \cdot \mathbf{k})\mathbf{k}}{k^2}, \quad (13)$$

$$\mathbf{v}_B(\mathbf{k}) = \mathbf{v}(\mathbf{k}) - \mathbf{v}_E(\mathbf{k}). \quad (14)$$

Traditionally, we present the measured E-mode velocity power spectrum

$$P_{vv}(k) = \langle \mathbf{v}_E \mathbf{v}_E^* \rangle \quad (15)$$

in the form of $\Delta_{vv}^2(k) = k^3 P_{vv}(k) / 2\pi^2$.

The velocity power spectra of the simulation samples with $f < 1$ should be statistically identical to that of the full sample ($f = 1$), if free of the sampling artifact. Furthermore, since these samples share the same cosmic variance as the full sample, their relative difference is free of cosmic variance. Therefore, the difference in the velocity power spectra of these samples should be interpreted as a sampling artifact. We perform the above test on three simulation snapshots, $z = 0, 1.07$, and 1.87 , to quantify the redshift dependence of Kriging II. We also compare Kriging I and Kriging II to see whether there is improvement by considering the anisotropy in the variogram.

IV. PERFORMANCE OF KRIGING II

For the variogram prior, we adopt the linear velocity divergence power spectrum $\Delta_{\theta\theta}^2$ generated by the CLASS code [33]. This is then used to calculate $\psi_{\perp}(r)$ and $\psi_{\parallel}(r)$ following Eqs. (6) and (7) and the result is shown in Fig. 1. $\xi_{\alpha\beta}(\mathbf{r})$ is calculated using Eq. (1), and the results of ξ_{xx} and ξ_{xy} are shown in Fig. 2. The correlation functions and therefore the variograms are clearly anisotropic.

The velocity power spectra obtained by Kriging II at $z = 0$, with the variogram specified above are presented by the dotted line in Fig. 3, for various f . We found that for the highest two sampling fraction cases (i.e., $f = 100\%$ and 10%), the resulting E-mode power spectra boost up abnormally at small scales. In these two cases, the Kriging system is found to be unstable for a large fraction of grid points. For these grid points, the resulting weighting does not satisfy $\sum_i W_i = 1$. However, most of the W_i are abnormally large. This implies that the Kriging system is almost degenerate for some velocity component(s) on these grid points. We also check the condition number for the matrix in Eq. (5), and it also implies that the matrix is ill conditioned.

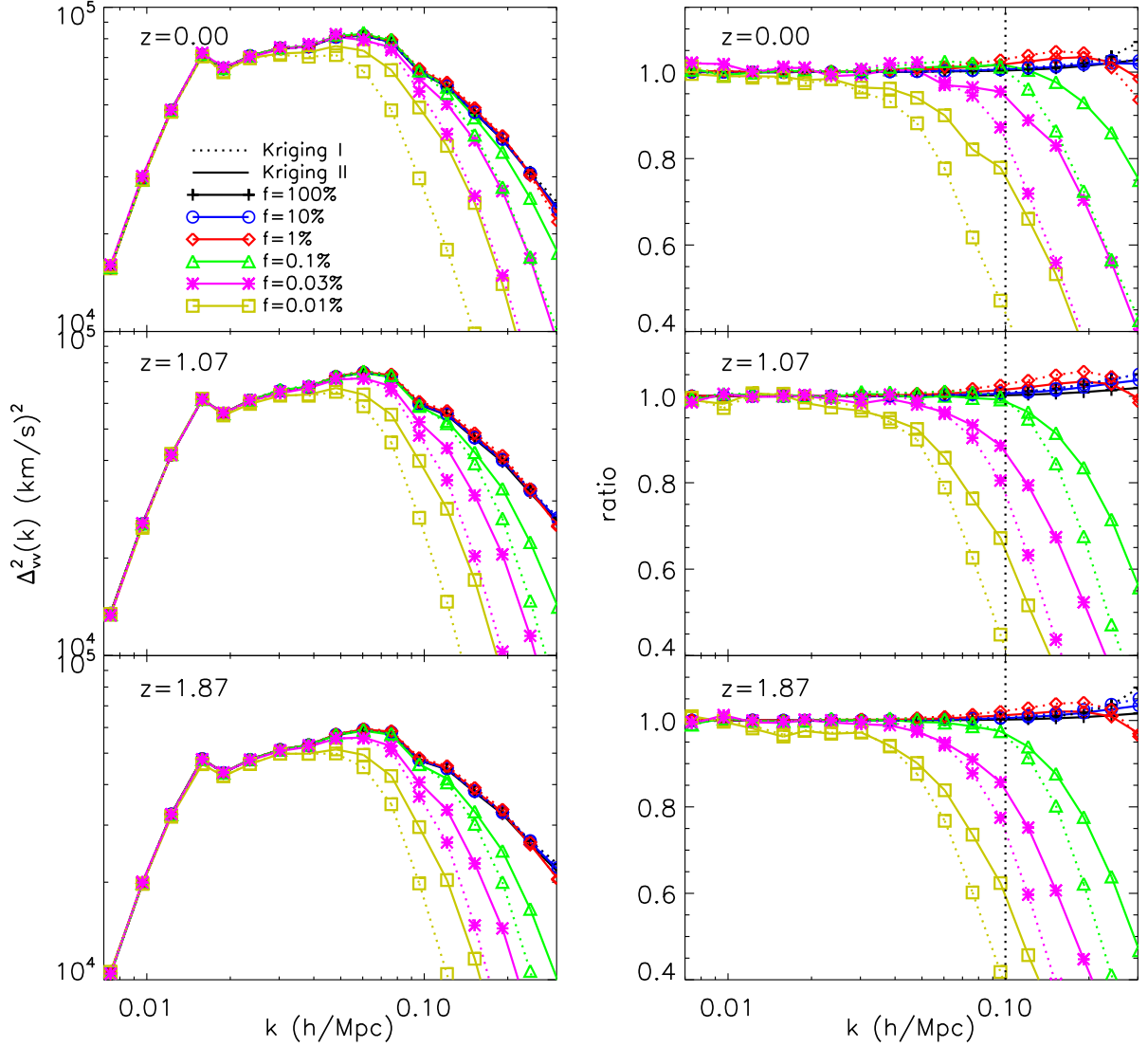


FIG. 4. E-mode velocity power spectrum from the Kriging method is presented in the left panel. The power from Kriging II is presented by solid lines, while the result of Kriging I is presented by dotted lines. Obvious improvement is observed. From top to bottom, the result for $z = 0, 1.07, 1.87$ is presented. The right panel presents the ratio to the reference cases. The vertical dotted line indicates the most concerned scale $k = 0.1 h\text{Mpc}^{-1}$.

The fact that this behavior only appears for the densest samples implies the possible cause of multi-streaming. Kriging II, with a variogram depending on the directions between the given grid point at \mathbf{x}_{grid} and nearby particles at $\mathbf{x}_{\text{grid}} + \mathbf{r}$, may lead to inconsistent solutions. For example, v_x information of nearby particles at positions $\mathbf{x}_{\text{grid}} + (r, 0, 0)$ contributes significantly to the reconstruction of $v_x(\mathbf{x}_{\text{grid}})$. Here, r is much smaller than the velocity correlation length. Particles at $\mathbf{x}_{\text{grid}} + (0, r, 0)$ also have comparable contribution. But due to multi-streaming, particles at $\mathbf{x}_{\text{grid}} + (r, 0, 0)$ and $\mathbf{x}_{\text{grid}} + (0, r, 0)$ can have very different v_x . Such differences can confuse Kriging II, leading to the observed degenerate Kriging system and the abnormal behavior found above.

To alleviate this problem, we include the nugget ef-

fect following Eq. (10), and try different values of the nugget parameter γ_{nug} . Overall, it causes suppression of small scale power, as expected if it is caused by multi-streaming. For $\gamma_{\text{nug}} = 0.001$, it solves the problem for $f = 10\%$ (Fig. 3), but the abnormal boost of power at the small scale still remains for the $f = 100\%$ case. For $\gamma_{\text{nug}} = 0.005$, it fully solves the problem for all the cases we consider. In contrast, it has a negligible effect on the cases of $f < 1\%$ and scales of $k \sim 0.1 h\text{Mpc}^{-1}$. This also supports our speculation that the nugget effect is related to multi-streaming. For low number density samples, there are essentially no close particle pairs. The above small scale multi-streaming induced problem will not happen. Hereafter, we will fix $\gamma_{\text{nug}} = 0.005$.

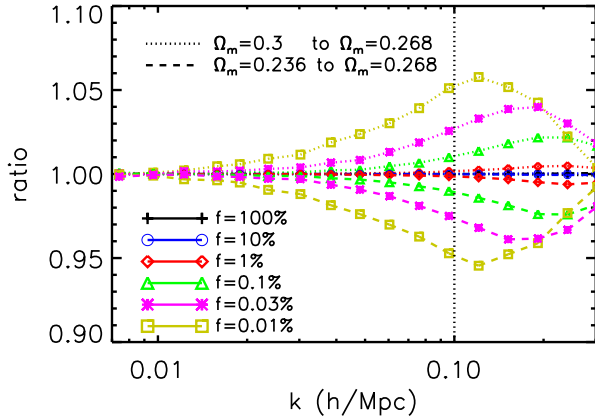


FIG. 5. E-mode velocity power spectrum deviations induced by adopting two inconsistent variograms predicted from a $\Omega_m = 0.3$ and $\Omega_m = 0.236$ flat universe. The vertical dotted line indicates the most concerned scale $k = 0.1 h\text{Mpc}^{-1}$. For $f = 0.1\%$, 0.03% , and 0.01% , the deviation is controlled at 1%, 3% and 5% level at $k = 0.1 h\text{Mpc}^{-1}$. Compared to the result in paper I, the sensitivity on the variogram prior is weakened by considering the more reasonable variogram in Kriging II.

A. Improvements by Kriging II

The $z = 0$ E-mode velocity power spectrum obtained by Kriging II is presented in the top panel of Fig. 4 by solid lines and is compared to that obtained by Kriging I (dotted lines). For low number density samples, the improvement of Kriging II over Kriging I is significant. The severe underestimation of small-scale power by Kriging I is significantly alleviated for $f = 0.1\%$, 0.03% , and 0.01% . For example, for $f = 0.01\%$, the $\sim 55\%$ underestimation at $k = 0.1 h\text{Mpc}^{-1}$ by Kriging I is reduced to $\sim 20\%$ by Kriging II. As a consequence, it expands the scale of reliable measurement by a factor of ~ 1.6 .

Another problem found in paper I is that the velocity statistics obtained by Kriging I has non-negligible dependence on the variogram, and this dependence is more severe for low number density samples. For example, if we change the variogram from that of the fiducial $\Omega_m = 0.268$ flat ΛCDM cosmology to a $\Omega_m = 0.3$ flat ΛCDM cosmology, the velocity power spectrum at $k = 0.1 h\text{Mpc}^{-1}$ changes by 2% for $f = 0.1\%$ and by 8% for $f = 0.01\%$ (Fig. 5, paper I). Kriging II still has such unsatisfactory dependence on variogram prior (Fig. 5). Nevertheless, it is much weaker, and the changes are 1% for $f = 0.1\%$ and 5% for $f = 0.01\%$. The dependence on the variogram prior is one major limiting factor of the cosmological application of Kriging. Therefore, although this problem is not fully solved, the improvement by Kriging II is a notable step forward.

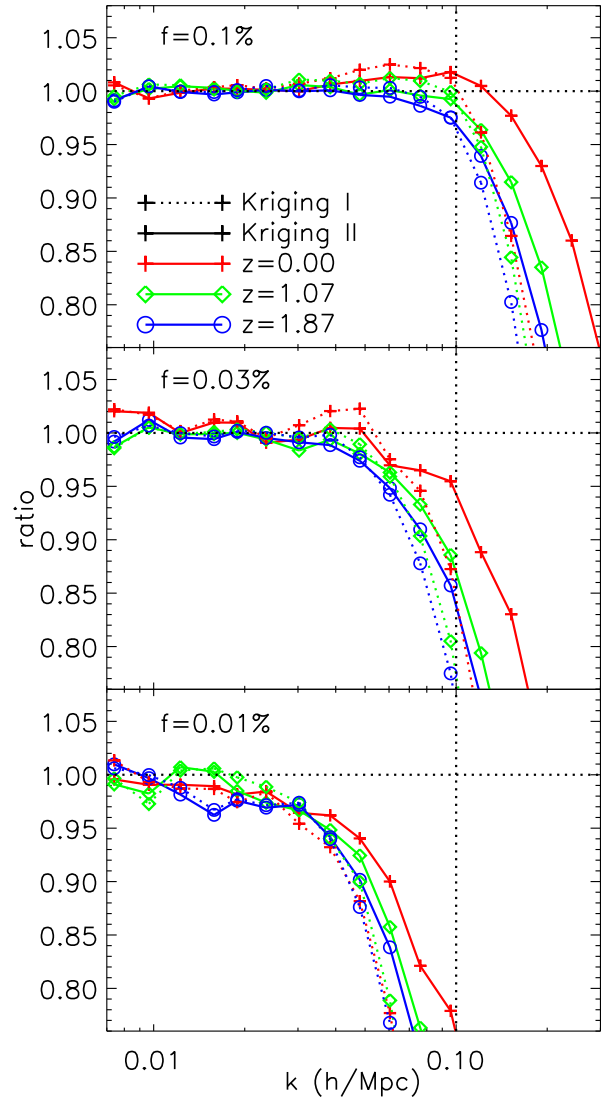


FIG. 6. We present the redshift dependence of the Kriging performance for $f = 0.1\%$, 0.03% , and 0.01% from top to bottom, respectively. For a given f , the ratio of the E-mode velocity power spectrum to the reference case is presented for both Kriging I (dotted line) and Kriging II (solid line). Both Kriging I and Kriging II perform better at lower redshift.

B. Redshift dependence

The improvement of Kriging II over Kriging I is also observed at other redshifts. Figure 6 shows the comparison at two arbitrarily chosen redshifts, $z = 1.07$ and 1.87 . In particular, for low number density samples, Kriging II produces a larger velocity power spectrum, closer to the correct result.

An interesting behavior of Kriging is that its performance is worse at higher redshift. This is likely related to the redshift dependences of two characteristic scales. As in paper I, we define the characteristic length for the

velocity field,

$$L_v = \left(\frac{\langle (\nabla \cdot \mathbf{v})^2 \rangle}{\langle v^2 \rangle} \right)^{-\frac{1}{2}}. \quad (16)$$

We then measure it from the full simulation sample with a negligible sampling artifact. This characteristic length describes the length on which the velocity field varies significantly. The measured L_v is 6.64, 6.00, and 5.83 $h^{-1}\text{Mpc}$ for $z = 0, 1.07, 1.87$, respectively. Another scale is the mean particle separation,

$$L_P = \frac{1200}{1024} f^{-1/3} h^{-1}\text{Mpc}. \quad (17)$$

The L_P values for decreasing f from $f = 100\%$, 10%, 1%, 0.1%, 0.03%, and 0.01% are 1.17, 2.52, 5.44, 11.7, and 25.3 $h^{-1}\text{Mpc}$, respectively.

To reliably sample the velocity field, we should have $L_P \lesssim L_v$. This condition is satisfied when $f \gtrsim 0.1\%$, but violated when $f \lesssim 0.1\%$ for all three redshifts we investigated. This explains that for all redshifts, the Kriging method suddenly fails for $f \lesssim 0.1\%$.

V. CONCLUSION AND DISCUSSION

Velocity assignment is a crucial ingredient of understanding the statistics of a cosmological velocity field. Motivated by the existence of a sampling artifact in existing velocity assignment methods, we introduced the Kriging method (Kriging I) in paper I. The current paper investigates physically motivated modifications of Kriging I. The modifications in Kriging II are an anisotropic variogram taking the anisotropy of velocity correlation into account and the nugget effect taking the multi-streaming into account. At $k = 0.1h\text{Mpc}^{-1}$ of interest, we find significant improvement for low number density samples.

Unfortunately, even the improved Kriging II still biases the velocity power spectrum at $k = 0.1h\text{Mpc}^{-1}$ by $\mathcal{O}(5)\%$ for samples of number density $\sim 10^{-4}\text{Mpc}^{-3}$. Such a systematic error is larger than the requirement from the stage IV dark energy projects. Therefore, further improvements are still required. We have tried other modifications in the framework of Kriging but found no

success. As a reference for possible future studies of Kriging as a velocity assignment method, we show one example. Kriging I and II interpolate one velocity component of nearby particles (e.g., v_x of particles) to obtain the same velocity component (e.g., v_x on the grid). Since $\xi_{\alpha\beta} \neq 0$ even when $\alpha \neq \beta$ (e.g., right panel of Fig. 2), we can Kriging interpolate v_y of nearby particles to obtain v_x on the grid. Such a version of Kriging is called the *Kolmogorov-Wiener prediction*. Thus, any data that correlate with the target data can be used to help the prediction. This is called *co-Kriging*. This uses more information of particle velocities and can in principle help the velocity assignment. We have tried co-Kriging, by extending the variogram matrix to include all α, β pairs. However, we found that this process is extremely unstable. For most of the grid points, the Kriging system is degenerate, unless extremely low $n_k \sim 5$ is adopted. Furthermore, even for such a low n_k , the smoothing effect of Kriging dominates, leading to a large suppression in the resulting power, as reported in paper I. Therefore, co-Kriging does not help for a practical situation.

We have also tried methods other than Kriging, NP, and tessellations. For example, we are looking for methods that can avoid the interpolation onto a regular grid. We have tried the nonuniform fast Fourier transform method [34]. Finally, we found that it essentially provides the mass-weighted velocity. Although it was a failed attempt, we present this negative result as a useful reference for future studies of better velocity assignment methods.

ACKNOWLEDGMENTS

This work was supported by the National Science Foundation of China (Grants No. 11403071, No. 11320101002, No. 11433001, No. 11621303, No. 11653003), National Basic Research Program of China (973 Programs No. 2013CB834900 and No. 2015CB857001), Key Laboratory for Particle Physics, Astrophysics and Cosmology, Ministry of Education, and Shanghai Key Laboratory for Particle Physics and Cosmology (SKLPPC). J.Z. is supported by the national Thousand Talents Program for distinguished young scholars and the T.D. Lee Scholarship from the High Energy Physics Center of Peking University. This work made use of the High Performance Computing Resource in the Core Facility for Advanced Research Computing at Shanghai Astronomical Observatory.

-
- [1] N. Kaiser, Mon. Not. R. Astron. Soc. **227**, 1 (1987).
 [2] J. A. Peacock, S. Cole, P. Norberg, C. M. Baugh, J. Bland-Hawthorn, T. Bridges, R. D. Cannon, M. Colless, C. Collins, W. Couch, G. Dalton, K. Deeley, R. De Propris, S. P. Driver, G. Efstathiou, R. S. Ellis, C. S. Frenk, K. Glazebrook, C. Jackson, O. Lahav, I. Lewis,

- S. Lumsden, S. Maddox, W. J. Percival, B. A. Peterson, I. Price, W. Sutherland, and K. Taylor, Nature (London) **410**, 169 (2001), astro-ph/0103143.
 [3] E. V. Linder and A. Jenkins, Mon. Not. R. Astron. Soc. **346**, 573 (2003), astro-ph/0305286.

- [4] P. Zhang, M. Liguori, R. Bean, and S. Dodelson, Phys. Rev. Lett. **99**, 141302 (2007), arXiv:0704.1932.
- [5] L. Guzzo, M. Pierleoni, B. Meneux, E. Branchini, O. Le Fèvre, C. Marinoni, B. Garilli, J. Blaizot, G. De Lucia, A. Pollo, H. J. McCracken, D. Bottini, V. Le Brun, D. Maccagni, J. P. Picat, R. Scaramella, M. Scodeggio, L. Tresse, G. Vettolani, A. Zanichelli, C. Adami, S. Arnouts, S. Bardelli, M. Bolzonella, A. Bongiorno, A. Cappi, S. Charlot, P. Ciliegi, T. Contini, O. Cucciati, S. de la Torre, K. Dolag, S. Foucaud, P. Franzetti, I. Gavignaud, O. Ilbert, A. Iovino, F. Lamareille, B. Marano, A. Mazure, P. Memeo, R. Merighi, L. Moscardini, S. Paltani, R. Pellò, E. Perez-Montero, L. Pozzetti, M. Radovich, D. Vergani, G. Zamorani, and E. Zucca, Nature (London) **451**, 541 (2008), arXiv:0802.1944.
- [6] B. Jain and P. Zhang, Phys. Rev. D **78**, 063503 (2008), arXiv:0709.2375.
- [7] Y. Wang, J. Cosmol. Astropart. Phys. **5**, 021 (2008), arXiv:0710.3885.
- [8] R. Reyes, R. Mandelbaum, U. Seljak, T. Baldauf, J. E. Gunn, L. Lombriser, and R. E. Smith, Nature (London) **464**, 256 (2010), arXiv:1003.2185 [astro-ph.CO].
- [9] M. Li, X.-D. Li, S. Wang, and Y. Wang, Communications in Theoretical Physics **56**, 525 (2011), arXiv:1103.5870.
- [10] T. Clifton, P. G. Ferreira, A. Padilla, and C. Skordis, Physics Reports **513**, 1 (2012), arXiv:1106.2476 [astro-ph.CO].
- [11] B. A. Reid, L. Samushia, M. White, W. J. Percival, M. Manera, N. Padmanabhan, A. J. Ross, A. G. Sánchez, S. Bailey, D. Bizyaev, A. S. Bolton, H. Brewington, J. Brinkmann, J. R. Brownstein, A. J. Cuesta, D. J. Eisenstein, J. E. Gunn, K. Honscheid, E. Malanushenko, V. Malanushenko, C. Maraston, C. K. McBride, D. Muna, R. C. Nichol, D. Oravetz, K. Pan, R. de Putter, N. A. Roe, N. P. Ross, D. J. Schlegel, D. P. Schneider, H.-J. Seo, A. Shelden, E. S. Sheldon, A. Simmons, R. A. Skibba, S. Snedden, M. E. C. Swanson, D. Thomas, J. Tinker, R. Tojeiro, L. Verde, D. A. Wake, B. A. Weaver, D. H. Weinberg, I. Zehavi, and G.-B. Zhao, Mon. Not. R. Astron. Soc. **426**, 2719 (2012), arXiv:1203.6641 [astro-ph.CO].
- [12] R. Tojeiro, W. J. Percival, J. Brinkmann, J. R. Brownstein, D. J. Eisenstein, M. Manera, C. Maraston, C. K. McBride, D. Muna, B. Reid, A. J. Ross, N. P. Ross, L. Samushia, N. Padmanabhan, D. P. Schneider, R. Skibba, A. G. Sánchez, M. E. C. Swanson, D. Thomas, J. L. Tinker, L. Verde, D. A. Wake, B. A. Weaver, and G.-B. Zhao, Mon. Not. R. Astron. Soc. **424**, 2339 (2012), arXiv:1203.6565 [astro-ph.CO].
- [13] D. H. Weinberg, M. J. Mortonson, D. J. Eisenstein, C. Hirata, A. G. Riess, and E. Rozo, Physics Reports **530**, 87 (2013), arXiv:1201.2434 [astro-ph.CO].
- [14] A. Joyce, B. Jain, J. Khoury, and M. Trodden, Physics Reports **568**, 1 (2015), arXiv:1407.0059.
- [15] K. Koyama, ArXiv e-prints (2015), arXiv:1504.04623.
- [16] P. Zhang and A. Stebbins, Physical Review Letters **107**, 041301 (2011), arXiv:1009.3967 [astro-ph.CO].
- [17] P. Zhang and M. C. Johnson, JCAP **6**, 046 (2015), arXiv:1501.00511.
- [18] P. Zhang, J. Pan, and Y. Zheng, Phys. Rev. D **87**, 063526 (2013), arXiv:1207.2722 [astro-ph.CO].
- [19] F. Bernardeau and R. van de Weygaert, Mon. Not. R. Astron. Soc. **279**, 693 (1996).
- [20] W. E. Schaap and R. van de Weygaert, Astron. Astrophys. **363**, L29 (2000), astro-ph/0011007.
- [21] Y. Zheng, P. Zhang, Y. Jing, W. Lin, and J. Pan, Phys. Rev. D **88**, 103510 (2013), arXiv:1308.0886 [astro-ph.CO].
- [22] J. Koda, C. Blake, T. Davis, C. Magoulas, C. M. Springob, M. Scrimgeour, A. Johnson, G. B. Poole, and L. Staveley-Smith, Mon. Not. R. Astron. Soc. **445**, 4267 (2014), arXiv:1312.1022 [astro-ph.CO].
- [23] P. Zhang, Y. Zheng, and Y. Jing, Phys. Rev. D **91**, 043522 (2015), arXiv:1405.7125.
- [24] Y. Zheng, P. Zhang, and Y. Jing, Phys. Rev. D **91**, 043523 (2015), arXiv:1409.6809.
- [25] E. Jennings, C. M. Baugh, and D. Hatt, Mon. Not. R. Astron. Soc. **446**, 793 (2015), arXiv:1407.7296.
- [26] Y. Yu, J. Zhang, Y. Jing, and P. Zhang, Phys. Rev. D **92**, 083527 (2015), arXiv:1505.06827.
- [27] This differs from another minimal variance linear estimator, the Wiener filter. The Wiener filter has a position independent window function.
- [28] P. J. E. Peebles, *Research supported by the National Science Foundation. Princeton, N.J., Princeton University Press, 1980. 435 p.* (Princeton University Press, NJ, 1980).
- [29] Y. P. Jing, Y. Suto, and H. J. Mo, Astrophys. J. **657**, 664 (2007), astro-ph/0610099.
- [30] <http://sci.esa.int/euclid/>.
- [31] <http://desi.lbl.gov/>.
- [32] <http://pfs.ipmu.jp/intro.html>.
- [33] <http://class-code.net/>.
- [34] <http://www.cims.nyu.edu/cmcl/nufft/nufft.html>.